Model-assisted CRISPRi/a library screening reveals central carbon metabolic targets for enhanced recombinant protein production in yeast

Metabolic Engineering 88 (2025) 1–13

Contents lists available at ScienceDirect

Metabolic Engineering

journal homepage: www.elsevier.com/locate/meteng

Model-assisted CRISPRi/a library screening reveals central carbon metabolic targets for enhanced recombinant protein production in yeast

Xin Chen [a,b,*], Feiran Li [a,c], Xiaowei Li [a], Maximilian Otto [a], Yu Chen [d], Verena Siewers [a,b,**]

[a] Division of Systems and Synthetic Biology, Department of Life Sciences, Chalmers University of Technology, SE-412 96, Gothenburg, Sweden
[b] Novo Nordisk Foundation Center for Biosustainability, Technical University of Denmark, DK-2800, Kgs. Lyngby, Denmark
[c] Institute of Biopharmaceutical and Health Engineering, Tsinghua Shenzhen International Graduate School, Tsinghua University, 518055, Shenzhen, China
[d] Key Laboratory of Quantitative Synthetic Biology, Shenzhen Institute of Synthetic Biology, Shenzhen Institute of Advanced Technology, Chinese Academy of Sciences, 518055, Shenzhen, China

ARTICLE INFO

Keywords:
Genome-scale model
CRISPRi/a library
Microfluidics
High-throughput screening
Recombinant protein production
Yeast cell factories

ABSTRACT

Production of recombinant proteins is regarded as an important breakthrough in the field of biomedicine and industrial biotechnology. Due to the complexity of the protein secretory pathway and its tight interaction with cellular metabolism, the application of traditional metabolic engineering tools to improve recombinant protein production faces major challenges. A systematic approach is required to generate novel design principles for superior protein secretion cell factories. Here, we applied a proteome-constrained genome-scale protein secretory model of the yeast *Saccharomyces cerevisiae* (pcSecYeast) to simulate α-amylase production under limited secretory capacity and predict gene targets for downregulation and upregulation to improve α-amylase production. The predicted targets were evaluated using high-throughput screening of specifically designed CRISPR interference/activation (CRISPRi/a) libraries and droplet microfluidics screening. From each library, 200 and 190 sorted clones, respectively, were manually verified. Out of them, 50% of predicted downregulation targets and 34.6% predicted upregulation targets were confirmed to improve α-amylase production. By simultaneously fine-tuning the expression of three genes in central carbon metabolism, i.e. *LPD1*, *MDH1*, and *ACS1*, we were able to increase the carbon flux in the fermentative pathway and α-amylase production. This study exemplifies how model-based predictions can be rapidly validated via a high-throughput screening approach. Our findings highlight novel engineering targets for cell factories and furthermore shed light on the connectivity between recombinant protein production and central carbon metabolism.

1. Introduction

Production of recombinant proteins is an important aspect in the fields of biomedicine and biotechnology (Gupta et al., 2017). Since human insulin was first produced from *Escherichia coli* in 1982, the US FDA has approved more than 130 recombinant proteins for clinical use and the annual growth rate of this market is estimated to be between 9.8% and 12.2% (Ow et al., 2021). The yeast *Saccharomyces cerevisiae* is one of the most prominent microbial workhorses for recombinant protein production (Vieira Gomes et al., 2018). The advantages of using *S. cerevisiae* as cell factory for recombinant protein production include 1) its rapid growth and easy genetic manipulation, 2) a eukaryal post-translational modification (PTM) machinery to facilitate proper protein function, 3) secretion of the target proteins to facilitate subsequent purification, 4) substantial information accumulated in the past, including databases and sequenced genomes (Madhavan et al., 2021). Protein synthesis and secretion are complex processes including transcription, translation, protein folding, translocation, different PTMs, endoplasmic reticulum (ER)-associated protein degradation, as well as vesicle transport. Many strategies have been investigated to optimize these processes and enhance recombinant protein production. Examples include selecting appropriate secretory signal peptides for extracellular targeting (Liu et al., 2012; Rakestraw et al., 2009), modifying the glycosylation pathway for heterologous protein expression (Claes et al.,

* Corresponding author. Division of Systems and Synthetic Biology, Department of Life Sciences, Chalmers University of Technology, SE-412 96, Gothenburg, Sweden.
** Corresponding author. Division of Systems and Synthetic Biology, Department of Life Sciences, Chalmers University of Technology, SE-412 96, Gothenburg, Sweden.
E-mail addresses: cxin@chalmers.se (X. Chen), siewers@chalmers.se (V. Siewers).

https://doi.org/10.1016/j.ymben.2024.11.010
Received 2 April 2024; Received in revised form 14 November 2024; Accepted 22 November 2024
Available online 29 November 2024

2024; Jacobs et al., 2009), regulating the unfolded protein response (UPR) to improve ER protein processing capacity and alleviate ER stress (Hetz and Papa, 2018; Lin et al., 2023), and enhancing vesicle trafficking from the ER to plasma membrane (Bao et al., 2017; Geva and Schuldiner, 2014) et al. In addition, metabolic processes interact closely with these processes by providing energy and precursors, coordinating redox homeostasis and signaling processes (Wang et al., 2017). A significant hurdle in optimizing yeast for enhanced recombinant protein production lies in harnessing its full cellular capabilities within its sophisticated secretory pathway and metabolic networks. Moreover, cell engineering to increase protein secretion has often relied on a trial-and-error approach, where various expression variables are being tested independently of each other. Consequently, the interactions between variables are neglected, rendering the trial-and-error process time-consuming (Cantoia et al., 2021; Ding et al., 2020). A more systematic approach is required to address this issue.

Systems biology can quantitatively describe cellular processes and predict gene targets for rational engineering of cell factories via genome-scale metabolic models (GEMs) (Nielsen, 2017). Traditional GEMs are extensively and successfully used for systematically simulating the cell metabolism and for rational cell factory design for production of various chemical compounds (Campbell et al., 2017; Cho et al., 2022; Zhang and Hua, 2015). In the context of recombinant protein production, the intricacies of the secretory pathway necessitate a comprehensive understanding of how cells manage biosynthetic costs and allocate cellular resources. However, prior research efforts have only offered partial insights into the secretory within metabolic models of yeast and other eukaryotes, failing to capture the intricate competition dynamics between recombinant and native secretory proteins. (Gutierrez et al., 2020; Irani et al., 2016; Krambeck and Betenbaugh, 2005). Recently, a proteome-constrained genome-scale protein secretory model for *S. cerevisiae* (pcSecYeast) was constructed, which integrates the traditional GEM and a description of the complete protein secretory pathway (Li et al., 2022). The integration of secretory and metabolic pathways in the pcSecYeast model can not only simulate the competition dynamics between recombinant proteins and native secretory proteins, but also offers insights into the metabolic and energetic demands associated with synthesizing recombinant proteins. Based on the characteristics of a recombinant protein, the model predicts gene targets specific to the production of this protein. In this study, the pcSecYeast model was leveraged to systematically identify potential gene targets within both secretory and metabolic pathways to enhance recombinant protein production.

Typically, the model can predict numerous gene targets for up- and downregulation, making it challenging to design a genetic engineering strategy that leads to the desired alteration in protein abundance, e.g. both transcription and translation efficiency would require to be taken into account. To comprehensively assess the predictive power of the pcSecYeast model, a CRISPR based metabolic engineering approach including interference/activation (CRISPRi/a) library can be applied to screen downregulated and upregulated gene targets, respectively (Cardiff et al., 2024; Gilbert et al., 2014; Johansson et al., 2023). CRISPRi/a relies on a catalytically inactive Cas9 (dCas9) with mutations in both the RuvC (D10A) and HNH (H840A) endonuclease domains, which can be exploited to modulate transcription through fusion with transcriptional repression and activation domains, e.g., the Mxi1 repressor for gene downregulation and the VP64-p65-Rta (VPR) tripartite activator for gene upregulation (Gilbert et al., 2014; Perez-Pinera et al., 2013). Unlike traditional gene knockdown or overexpression, CRISPRi/a modulates gene transcription without modifying the genome of the host organism (Bendixen et al., 2023). In addition, the gene expression level can be fine-tuned by choosing multiple gRNA sites in the target gene promoters (Ferreira et al., 2019). Typically, CRISPRi/a based approaches use genome-wide libraries (Cardiff et al., 2024). Here, we design specific libraries based on the model prediction, which allows testing a high number of gRNA targets per promoter.

It is a particular challenge to connect a genotype to a phenotype when screening libraries for secreted products, as in the case of recombinant protein production. Recently, droplet microfluidics has emerged as a powerful technology for high-throughput screening of single cells (Tran et al., 2013). This technology allows the single cell and its secreted product to be contained inside the droplet and has been used for various applications, including directed evolution of enzymes, large-scale gene assembly, and measurement of extracellular metabolites concentration (Chan et al., 2017; Huang et al., 2015; Mastrobattista et al., 2005). Generally, the single cell is encapsulated within single emulsion (SE) (water-in-oil) droplets, in which the aqueous droplet is surrounded by a hydrophobic oil phase (Baret et al., 2009). However, these SE droplets can only be screened via fluorescence-activated droplet sorting (FADS), which requires extensive instrumentation and specialized training to acquire the expertise for operation. A promising alternative is to encapsulate the single cell within double emulsions (DE) (water-in-oil-in-water), where the DE droplets are suspended in aqueous solution and which is compatible with a standard fluorescence-activated cell sorting (FACS) instrument (Brower et al., 2020a).

Here, we employed the pcSecYeast model to predict targets for increasing secretion of α-amylase in yeast cells and evaluated the targets by combining CRISPRi/a library and high-throughput DE droplet microfluidics screening (Fig. 1). Through systematic analysis and experimental verification, gene targets involved in diverse biological processes were identified, including central metabolism, PTMs and protein transport, which not only illustrated novel metabolic engineering targets for rational design of yeast cell factories, but also led to a better understanding of protein production mechanisms in yeast. Using dCas9-mediated multiplexed gene regulation, the expression of gene targets in the central carbon metabolism was fine-tuned to enhance fermentation process and generate strains with improved α-amylase production capability.

2. Results

2.1. pcSecYeast model prediction of gene targets for improved recombinant protein production

The enzyme α-amylase, composed of 478 amino acids and featuring four disulfide bonds, was utilized as a model recombinant protein in this study. To comprehensively assess the predictive capability of the pcSecYeast model, we used the model to predict both overexpression and downregulation targets for increased α-amylase production using an adapted Flux Scanning based on Enforced Objective Function (FSEOF) method (Fig. 2). Using this algorithm, a series of simulations was conducted to strategically improve α-amylase production by progressively decreasing the biomass yield from glucose. In each simulation, protein abundances within the pcSecYeast model were calculated, with the primary objective of maximizing α-amylase production. Genes that exhibited simultaneous increases in corresponding protein abundance alongside α-amylase enhancement were designated as overexpression targets, while those with opposing alterations were categorized as downregulation targets. The predicted overexpression and downregulation targets were ranked with priority scores based on the correlation confidence. By setting the cutoff of priority scores, 81 predicted overexpression targets (priority scores $\geq$3) and 76 predicted downregulation targets (priority scores ≤ -3) were selected (Supplementary Table 1).

2.2. CRISPRi/a library construction and droplet microfluidic screening

The *S. cerevisiae* strain CEN.PK 11C-GK1 was selected as a starting strain, where 14 copies of an α-amylase gene were integrated into chromosomal delta (δ) sites by repetitive transformation (Wang et al., 2019). This integration strain demonstrated α-amylase production comparable to the AAC strain, which expresses α-amylase using the

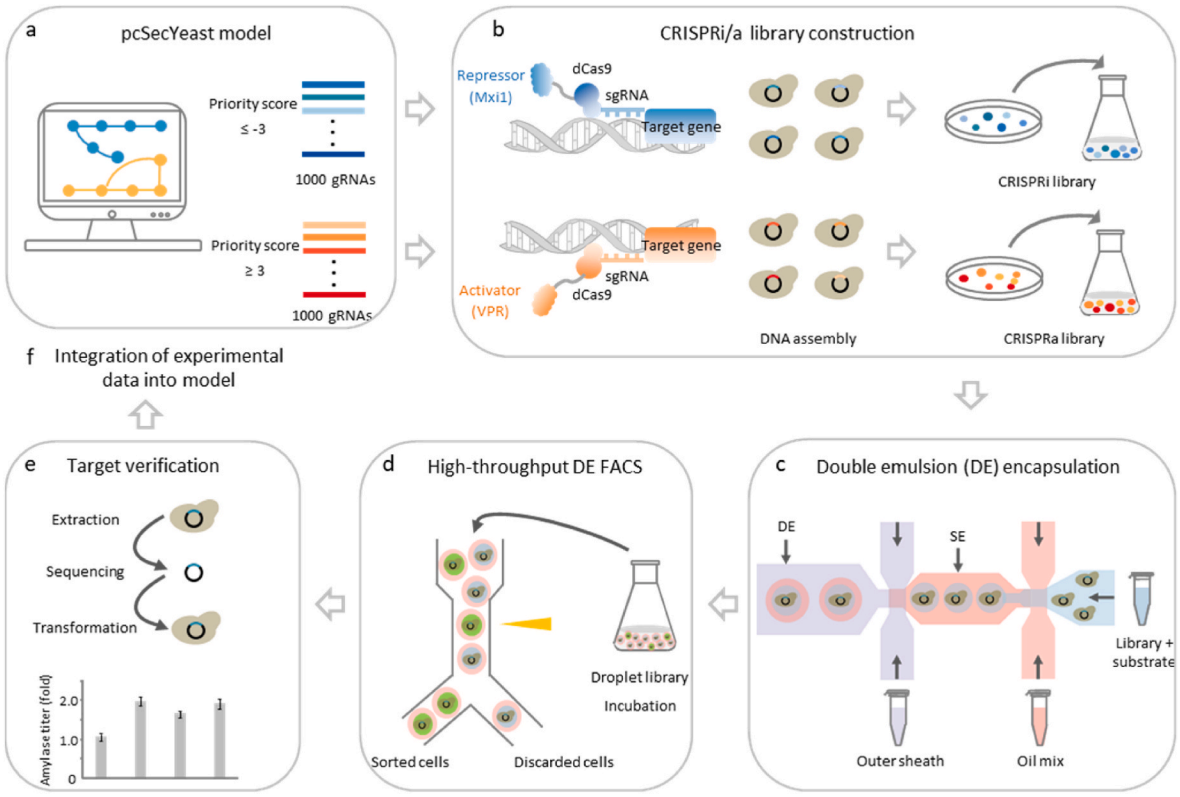

Fig. 1. Schematic workflow for genome-scale model-assisted high-throughput CRISPRi/a screening of *S. cerevisiae* to improve recombinant protein production. **a** The pcSecYeast model predicted a list of downregulation targets (priority score ≤ -3) and upregulation targets (priority score ≥ 3) to enhance α-amylase production. Two gRNA libraries with 1000 gRNAs each were designed to target downregulation and upregulation targets. **b** The two gRNA libraries were introduced into CRISPR-dCas9-Mxi1 and CRISPR-dCas9-VPR strains, respectively, to reduce or increase the expression of target genes. **c** The CRISPRi/a libraries were mixed with BODIPY labeled starch substrate and loaded into a microfluidic chip, resulting in the encapsulation of single cells within double emulsion (DE) droplets (water-oil-water). SE indicates single emulsion and DE indicates double emulsion. **d** The DE droplets were screened using FACS for fluorescence intensity, and strains with higher α-amylase production were sorted. **e** Plasmids from sorted clones were sequenced and their α-amylase production capacity was assessed. **f** The experimental data were integrated into the pecSecYeast model.

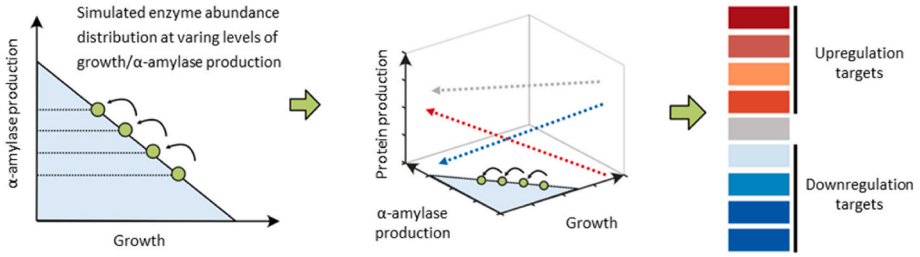

Fig. 2. Prediction of gene targets for α-amylase overproduction via the pcSecYeast model. An adapted Flux Scanning based on Enforced Objective Function (FSEOF) method was applied to identify gene targets. By simulation of progressively decreased cell growth, cells diverted carbon flow from growth to the maximal α-amylase production. The native protein abundances were calculated from each simulation. The proteins with increased abundance alongside α-amylase enhancement were categorized as upregulation targets, while those with decreased abundance were designated as downregulation targets.

CPOTud high-copy plasmid system (Huang et al., 2015) (Supplementary Fig. 1). Moreover, the integration strain ensures the stable expression of α-amylase and maintains consistency across cell generations. For stable expression, genes encoding dCas9 coupled to the Mxi1 repressor domain or dCas9 coupled to the VPR activator domain were chromosomally integrated into CEN.PK 11C-GK1. Based on the distance and orientation to the transcription start site or interference with other transcription factors, the dCas9 complex binding may generate graded transcriptional patterns (Anderson and Voigt, 2021). Therefore, up to 14 gRNAs per target gene promoter were designed to achieve a sufficiently broad regulatory spectrum. The CRISPRi library of 1000 gRNAs targeting 76 downregulation targets (Supplementary Table 2) and CRISPRa library of 1000 gRNAs targeting 81 overexpression targets (Supplementary Table 3) were cloned into a high-copy plasmid under the constitutive RNA polymerase III promoter (*SNR52p*) (Supplementary Fig. 2). The library coverage was evaluated through sequencing the plasmids from random transformants. Out of 20 screened clones, 19 different gRNA encoding sequences were detected in both the CRISPRi library and CRISPRia library (Supplementary Tables 4 and 5).

To capture clones with improved α-amylase production, a DE microfluidic system was established to screen for increased secreted α-amylase levels from individual cells at high throughput (Supplementary Fig. 3). Individual cells of the library were encapsulated in ~ 45 μm DE droplets along with a fluorogenic α-amylase substrate as a

reporter (Supplementary video). The level of fluorescence generated from hydrolyzed substrate correlates to the level of α-amylase within the droplets. After 3 h of incubation, approximately 50,000 DE droplets from each library were screened using FACS, a quantity fifty times larger than the library size to ensure sufficient coverage. The top 5% DE droplets with the highest fluorescence intensity were then sorted (Supplementary Fig. 4), and mixed cells from these droplets were plated on agar plates containing 1% starch as the sole carbon source. The α-amylase enzyme belongs to a family of endo-amylases that hydrolyze the α-1,4-glycosidic bonds of starch and release maltose and glucose for cell growth (Tangphatsornruang et al., 2005). Only cells secreting α-amylase can grow on these starch plates. This additional selection step is expected to help reduce the occurrence of false positives in our high-throughput screening.

The sorted cells were then individually verified by measuring α-amylase production in the supernatant after tube cultivation. From either library, 200 and 190 sorted cells were evaluated, respectively. Out of the analyzed clones, 81 clones (40.5%) from the CRISPRi library and 65 clones (34.2%) from the CRISPRa library significantly improved α-amylase titer compared with the control strain ($p < 0.05$, fold of α-amylase titer ≥1.2, Fig. 3a and c). These results demonstrate that the combination of microfluidic droplet encapsulation and FACS is a viable strategy for high-throughput screening of CRISPR/dCas9 gRNA library to improve α-amylase production.

2.3. Characterization of sorted CRISPRi/a gene targets

The gRNA encoding plasmids were extracted from 81 strains from the CRISPRi library and 65 strains from the CRISPRa library. Subsequent sequencing results covered 38 and 28 gene targets of the CRISPRi and CRISPRa libraries, respectively (Supplementary Tables 6 and 7). Of the 38 verified target genes from the CRISPRi library, 7 genes (*IDP1*, *TDH3*, *PGI1*, *IMD4*, *MET13*, *MEP3*, *GLN1*) were targeted by 3 different gRNAs each, while among the 28 genes from CRISPRa library, 5 genes (*PDI1*, *OCH1*, *TRS31*, *HOC1*, *SEC16*) were targeted by 3 different gRNAs each. For the remaining target genes, 1–2 different gRNAs were identified.

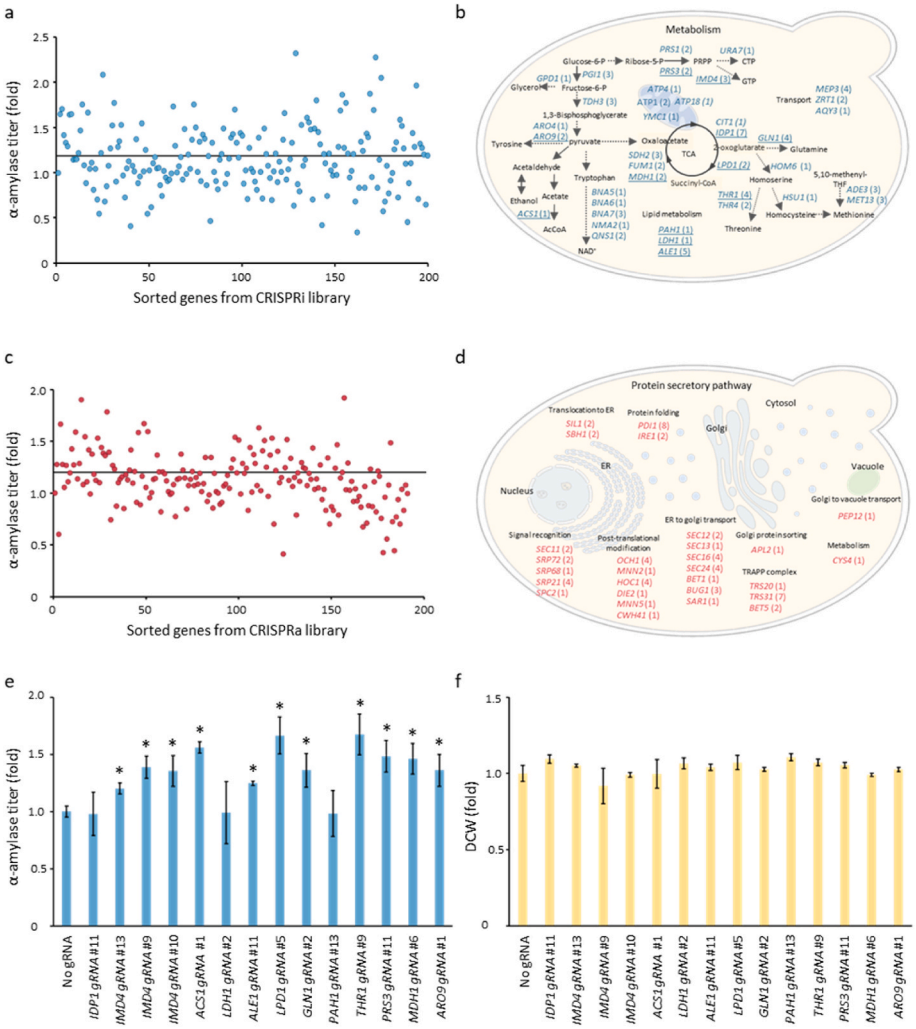

Fig. 3. Experimental assessment of library clones after droplet sorting. **a** Normalized α-amylase production of 200 clones from the sorted CRISPRi library. **b** Downregulated targets with significantly increased α-amylase production mapped to metabolic pathways ($p < 0.05$, α-amylase titer ≥1.2-fold). The 14 target genes from the strains with the highest α-amylase production (α-amylase titer ≥1.5-fold) are underlined. **c** Normalized α-amylase production of 190 clones from the sorted CRISPRa library. Each dot in (**a**) and (**c**) represents data from an individual strain. The black line in (**a**) and (**c**) marks the cutoff value of 1.2 of the fold of α-amylase titer. **d** Upregulated targets with significantly increased α-amylase production mapped to the secretory pathway ($p < 0.05$, α-amylase titer ≥1.2-fold). The numbers in (**b**) and (**d**) indicate the number of gRNAs identified for the individual genes. These gRNAs could be the same or different ones. **e** and **f** Reverse engineering to verify the effect of the 14 gRNAs strains from (**b**) on α-amylase production. The gRNA expression plasmids were extracted from these strains and re-transformed into the parental strain to validate their efficacy on α-amylase production (**e**) and dry cell weight (DCW) (**f**). The results from (**e**) and (**f**) show the average values ± SD from four independent biological replicates. Asterisks (*) indicate significant differences compared to control strain without gRNA expression ($p < 0.05$).

Depending on the gRNA target sites, CRISPRi/a regulation showed different impact on α-amylase production. For instance, *OCH1* gRNA #3, #12 and #7 increased the α-amylase titer by 20%, 43%, and 90%, respectively (Supplementary Table 7).

In total, 38 out of 76 predicted downregulation targets (50%) were validated as positive targets, while 28/81 (34.6%) of the predicted overexpression targets were obtained (Fig. 3b and d). The gene set enrichment analysis (GSEA) showed that verified downregulation targets were significantly enriched in metabolism-associated genes, including carbon metabolism, tricarboxylic acid (TCA) cycle, biosynthesis of amino acids and nicotinamide adenine dinucleotide (NAD) (FDR <0.05, Supplementary Fig. 5a and Supplementary Table 8). On the other hand, the confirmed overexpression targets were significantly enriched in genes associated with the secretory pathway spanning post-translational modification (PTM) and protein transport (FDR <0.05, Supplementary Fig. 5b and Supplementary Table 9). Among the verified downregulation targets, only *MDH1*, which encodes the mitochondrial malate dehydrogenase in the TCA cycle, has been shown to enhance human superoxide dismutase (hSOD) production upon the plasmid-based gene overexpression in *Pichia pastoris* (Nocon et al., 2014). The capacity of the secretory pathway is commonly observed as a bottleneck for recombinant protein secretion. As a result, significant efforts have been dedicated to relieving this bottleneck by regulation of genes involved in this pathway to boost protein production. Nine out of these verified upregulation targets have been validated for enhancing the production of various recombinant proteins in previous studies (Supplementary Table 10). These targets' functions are associated with protein folding and ER stress (*PDI1*, *IRE1*, *CWH41*), protein translocation (*SEC16*, *SBH1*, *SIL1*), PTMs (*OCH1*, *HOC1*), and cysteine biosynthesis (*CYS4*) (Supplementary Table 9). The high accuracy of the pcSecYeast model predictions demonstrates the value of the presented mathematical model for systematic analysis of complex cellular metabolism and the protein secretory pathway in recombinant protein production. The GSEA results indicate that, in line with the secretory pathway, targeting metabolism may be equally important for improving recombinant protein production. It is in accordance with previous findings, showing that efficient protein production is associated with global tuning of cellular metabolism (Chen et al., 2022; Huang et al., 2017). However, these studies did not provide a detailed description of the relationship between metabolism and protein production. Given the limited studies on metabolic targets in this context, our focus was directed towards these targets in the subsequent study.

2.4. Characterization of central carbon metabolic targets for improved protein production

From the identified and verified downregulation targets, 14 strains with the best performance in α-amylase production (α-amylase titer ≥1.5-fold) were selected for reverse engineering. The gRNA plasmids were extracted from these strains and re-transformed into the 11C-GK1-dCas9-Mxi1 parental strain to validate their efficacy on α-amylase production. Out of 14 strains, 11 strains showed improved α-amylase production, including *IMD4* gRNA #9, #10 and #13, *ACS1* gRNA #1, *ALE1* gRNA #1, *LPD1* gRNA #5, *GLN1* gRNA #2, *THR1* gRNA #9, *PRS3* gRNA #11, *MDH1* gRNA #6 and *ARO9* gRNA #1 (Fig. 3e and f). Furthermore, all of these genes, with the exception of essential genes *GLN1* and *THR1*, were individually deleted to evaluate their impact on α-amylase production. None of the gene deletions showed a promotive impact on α-amylase production, with 2 deletion strains (*lpd1Δ* and *mdh1Δ*) resulting in significantly decreased α-amylase production compared to the control strain (Supplementary Fig. 6a). This illustrates the importance of fine-tuning gene expression to improve recombinant protein production.

Notably, the *lpd1Δ* and *mdh1Δ* strains displayed growth defects on ethanol (Supplementary Fig. 7), and their final biomass was significantly reduced to 1.51 g L^{-1} and 1.86 g L^{-1}, compared to 3.65 g L^{-1} in the control strain (Supplementary Fig. 6b). Both *LPD1* and *MDH1* are involved in the TCA cycle. The *LPD1* gene encodes the lipoamide dehydrogenase subunit of pyruvate dehydrogenase and the 2-oxoglutarate dehydrogenase complex, while the *MDH1* gene encodes malate dehydrogenase that converts malate to oxaloacetate (Fig. 4a). Even though these TCA cycle genes are nonessential on glucose, mutant strains display various growth defects on nonfermentable carbon sources, such as ethanol, acetate, and glycerol (Przybyla-Zawislak et al., 1999), which may explain the decreased biomass and α-amylase production in *lpd1Δ* and *mdh1Δ* strains (Supplementary Fig. 6). As a Crabtree-positive organism, *S. cerevisiae* employs fermentative pathways to rapidly metabolize glucose and generate ethanol even under aerobic conditions (glucose phase). When glucose is consumed, cells transit to the respiratory pathway to utilize ethanol after the diauxic shift. Research indicates that altering energy metabolism to favor increased fermentation

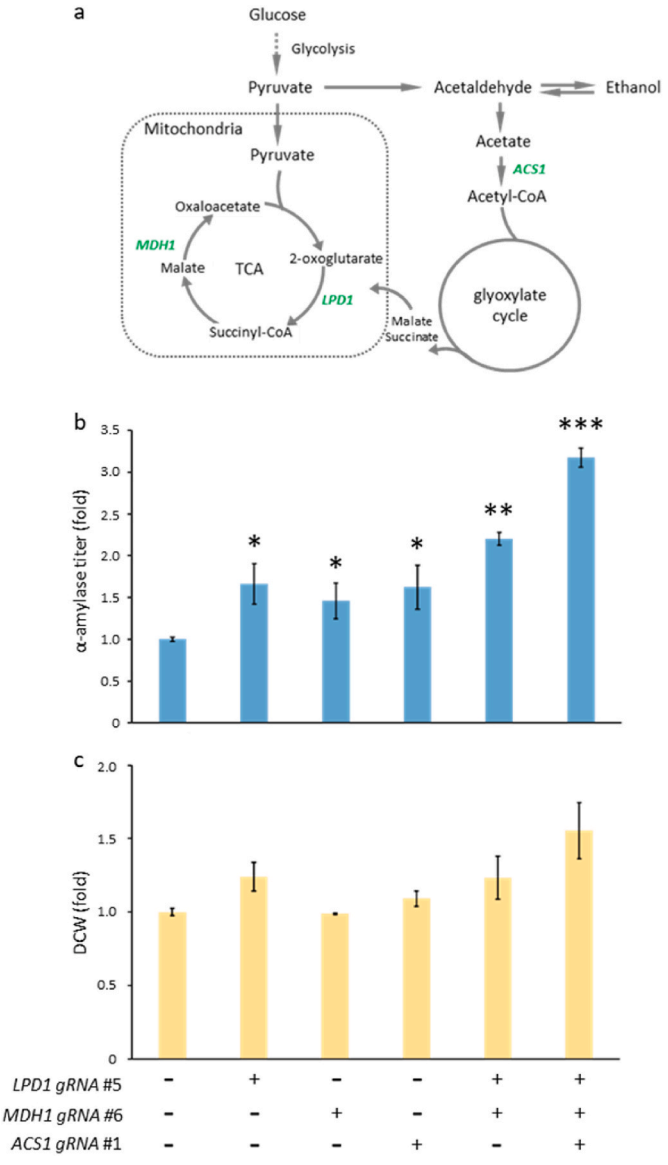

Fig. 4. Combinatorial fine-tuning of gene expression for improved α-amylase production. **a** Schematic overview of engineered gene targets in the central carbon metabolism. The α-amylase titers (**b**) and DCW (**c**) of engineered strains with down-regulated expression of *LPD1*, *MDH1*, and *ACS1* via dCas9-Mix1 were assessed. Asterisks (*) indicate significant differences compared to the control strain ($p < 0.05$). The results show the average values ± SD from four independent biological replicates. *$p < 0.05$; **$p < 0.01$ compared to control strain without gRNA expression.

has been shown to effectively enhance recombinant protein production (Huang et al., 2015, 2017). Downregulation of *LPD1* and *MDH1* may enhance carbon flux to fermentation to meet the increased energy demand at higher α-amylase production. Furthermore, the *ACS1* gene encodes acetyl-CoA synthetase that converts acetate to acetyl-CoA. Repression of *ACS1* expression may divert the carbon flux from acetate consumption to ethanol production in the fermentative pathway for enhanced α-amylase production (Figs. 3e and 4a). Therefore, the *LPD1* gRNA #5, *MDH1* gRNA #6, and *ACS1* gRNA #1 were chosen for combinatorial evaluation of their effects.

2.5. Redistribution of central carbon fluxes for increased protein production

To generate multiple gRNAs from a single transcript to control the expression of multiple genes at the same time, we employed the Csy4 endonuclease (Ferreira et al., 2018) (Supplementary Fig. 8a). Co-expression of *LPD1* gRNA #5 and *MDH1* gRNA #6 led to a 2.20-fold α-amylase production compared to control strain. This was significantly higher than production by the individual *LPD1* gRNA #5 and *MDH1* gRNA #6 repression strains, which was 1.66-fold and 1.46-fold compared to control strain (Fig. 4b and Supplementary Fig. 8b). Thereafter, *ACS1* gRNA #1 was expressed in the *LPD1* #5 and *MDH1* #6 combinatorial strain to downregulate the expression of all 3 genes simultaneously (Supplementary Fig. 8c). This triple-gRNA combination

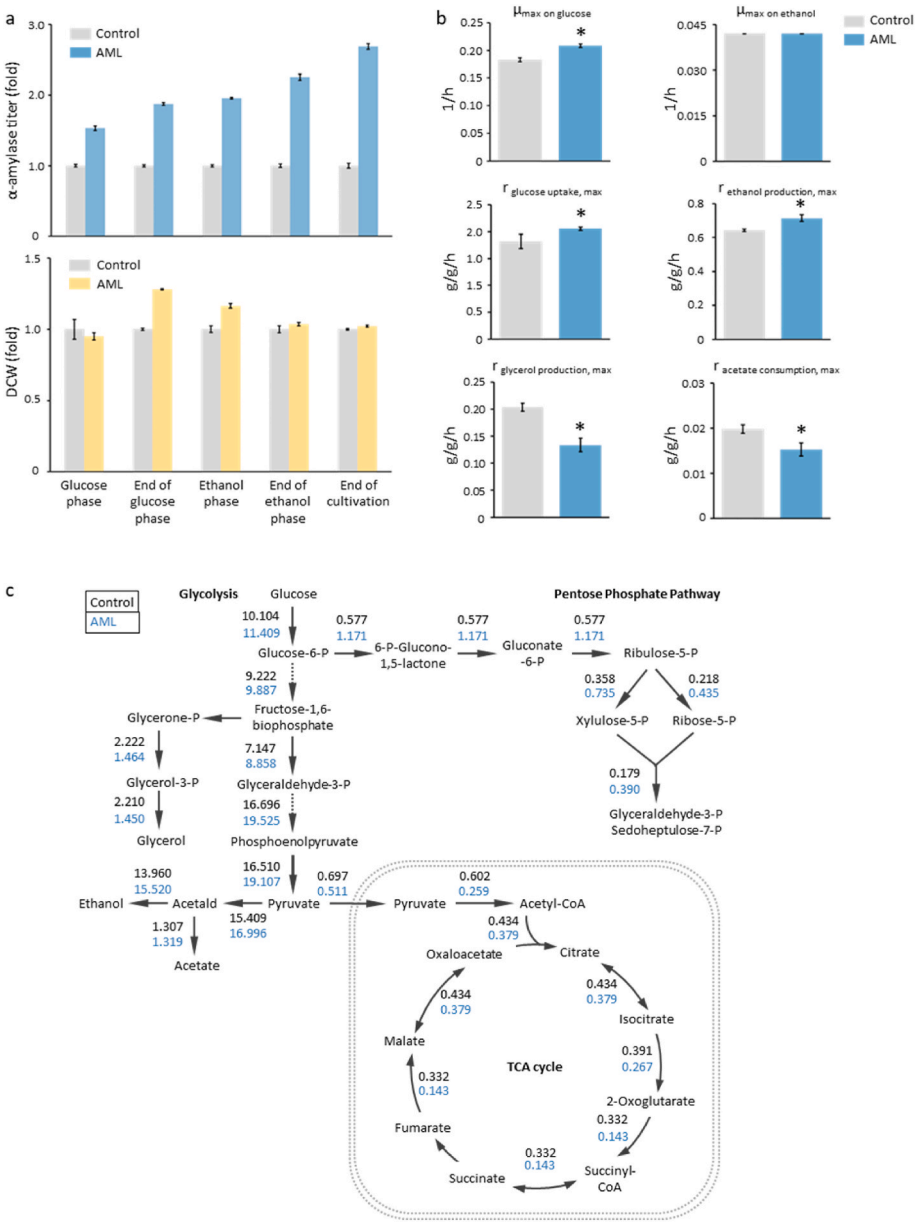

Fig. 5. Characterization of the best performance strain AML and control strain in shake-flask cultivation. **a** The α-amylase titers and DCW over time. **b** Physiological parameters. $\mu_{max\ on\ glucose}$: maximal biomass-specific growth rate on glucose; $\mu_{max\ on\ ethanol}$: maximal biomass-specific growth rate on ethanol; $r_{glucose\ uptake,\ max}$: maximal biomass-specific glucose consumption rate; $r_{ethanol\ production,\ max}$: maximal biomass-specific ethanol production rate; $r_{glycerol\ production,\ max}$: maximal biomass-specific glycerol production rate; $r_{acetate\ consumption,\ max}$: maximal biomass-specific acetate consumption rate. **c** FBA prediction of metabolic flux distributions in the central carbon metabolism for control strain (in black color) and AML strain (in blue color). (For interpretation of the references to color in this figure legend, the reader is referred to the Web version of this article.)

further enhanced α-amylase production to 3.18-fold (Fig. 4b). This result was confirmed by SDS/PAGE analysis of supernatant from cultures (Supplementary Fig. 9). In this best performing strain (hereafter referred to as AML strain), the mRNA levels of *LPD1*, *MDH1*, and *ACS1* were decreased by 57%, 30%, and 22%, respectively (Supplementary Fig. 10). These results indicate that fine-tuning expression of multiple genes via dCas9-mediated CRISPRi/a acts as an effective tool for improved protein production.

To explore the diversion of carbon flux distribution after the triple-gene modifications, the physiological properties of the AML and control strains were characterized in shake-flask cultivation. The AML strain showed an improved α-amylase titer throughout the whole cultivation process compared to the control strain (Fig. 5a). There was no significant effect on final biomass formation in the AML strain (Table 1 and Supplementary Fig. 11), which was different from previous studies in which increased protein production is usually accompanied by reduced biomass formation (Chen et al., 2022; Huang et al., 2017, 2018). These studies used gene deletion or plasmid-based gene overexpression system as modification tools. The AML strain showed a 11.5% increase in specific glucose uptake rate and a 12.5% increase in maximum specific growth rate during the glucose phase. The AML strain also showed slower byproduct formation, i.e., a 34.3% decrease in the specific glycerol production rate. The 25% decrease in specific acetate consumption rate in the AML strain could be associated to the down-regulation of *ACS1* that slows down the conversion of acetate to acetyl-CoA. Relative to the reduction in specific glycerol production rate, an increased specific production rate (10.1%) and yield (7.0%) of ethanol, a carbon source for the post-diauxic phase, were discovered in the AML strain (Fig. 5b and Table 1). This was in accordance with our combinatorial gene regulations that should divert glycolytic flux towards ethanol production (Fig. 4a). Furthermore, flux balance analysis (FBA) confirmed that carbon flux was redistributed among glycolysis, TCA cycle, and pentose phosphate pathway (PPP) in the AML strain, compared to the control strain (Fig. 5c). The glycolytic flux was diverted from glycerol production and TCA cycle towards ethanol production. Consistently, the carbon flux through the PPP was increased, which may generate more reducing power (NADPH) for α-amylase overproduction. The carbon flux towards amino acid biosynthesis and tRNA synthetases was significantly increased in the AML strain compared to the control strain (Supplementary Fig. 12), which was previously shown to be favorable for protein production (Wu, 2009).

3. Discussion

The global market for recombinant proteins is expected to witness significant growth over the forecast period 2023 to 2032, reaching 8.95 billion-dollar by 2032. However, rational design of cell factories for recombinant protein production is a difficult task due to the complexity of the protein secretory pathway. The pcSecYeast model serves as a platform for systematic modeling of the secretory pathway and its connection with cellular metabolism. By analyzing the characteristics of a heterologous recombinant protein, this model can simulate the production of this protein to forecast how cells allocate their limited resources efficiently through regulatory networks, and identify gene targets specific to the production of this recombinant protein (Li et al., 2022).

Attaching inhibitory or activating domains to the dCas9 protein enables genome-scale analysis of gene function via CRISPRi or CRISPRa, which can reveal novel phenotypes and enables more flexible experimental designs. CRISPRi serves as a powerful tool for studying cellular physiology under different growth conditions, allowing for partial loss-of-function of essential genes (Evers et al., 2016; Silvis et al., 2021). Recently, a *S. cerevisiae* CRISPRi library has been screened for gene targets that regulate cellular tolerance to acetic acid stress, including more than 98% of essential and respiratory growth-essential genes (Mukherjee et al., 2021). A genome-scale CRISPRi library has proven effective in interrogation of gene function and interaction in *S. cerevisiae* (Momen-Roknabadi et al., 2020). CRISPRa libraries are suited for identifying alterations that promote cell survival, proliferation, and drug resistance genes in response to anticancer drug treatment (Legut et al., 2022; Ye et al., 2022). Based on the positioning and efficiency of the gRNA, varying levels of repression or activation can be evaluated by testing multiple gRNA sequences for each target gene (Smith et al., 2016). Through simulating specific recombinant protein production, our study was able to narrow down the number of gene targets, which allows for more precise and fine-tuned gene expression, utilizing up to 14 gRNAs per target (Supplementary Tables 2 and 3).

Precisely tuning gene expression is crucial for building microbial cell factories with higher titers and productivity. This process helps to minimize the accumulation of toxic metabolites, to decrease competition between cell growth and product production, and to balance the cofactor system (Jung et al., 2021). In previous studies, fine-tuning of gene expression and/or protein activity has traditionally relied on random mutagenesis methods to select strains with overproduction of compounds of interest. This can be achieved through chemical mutagens or physical mutagens like UV light or plasma (Cho et al., 2022; Huang et al., 2015; Ottenheim et al., 2018). However, the drawbacks of random mutagenesis include: 1) the necessity for a substantial number of mutants to cover the entire genome; 2) mutations being randomly distributed across the genome; 3) challenges in identifying causal mutation sites for a specific gene; and 4) the potential for accumulated mutations to hinder cell growth and genetic stability. In our engineered library using the CRISPRi or CRISPRa approach, alterations were precisely targeted to specific genes, with each strain containing only a single alteration (Supplementary Tables 4 and 5), making isolation and identification easier. Furthermore, these alterations did not affect cell growth (Supplementary Tables 6 and 7), potentially decreasing the likelihood of evolutionary pressure to eliminate them.

In order to effectively validate the CRISPR-based transcriptional regulation libraries, our study integrated the droplet microfluidic screening with high-throughput FACS sorting. Following sorting, 200 clones from CRISPRi library and 190 clones from CRISPRa library were manually analyzed. Among these, 38 out of 76 (50%) predicted down-regulation targets and 28 out of 81 (34.6%) of predicted upregulation targets were confirmed to be positive for α-amylase overproduction (Fig. 3b and d). Previous studies have not verified that downregulation of any of these 38 identified targets leads to an increase in recombinant protein production. Nevertheless, the repression of two identified upregulation targets, *OCH1* and *HOC1*, has shown beneficial effects on recombinant protein production in *Pichia pastoris* (Supplementary Table 10). Although yeasts can carry out various human PTM reactions,

Table 1
Physiological characterization of the control strain and AML strain.

Strain	Control	AML
$Y_{x/s}$ (g/g)[a]	0.26 ± 0.01	0.27 ± 0.01
$Y_{ethanol/s}$ (mCmol/Cmol)[b]	465.58 ± 20.12	500.56 ± 7.94*
$Y_{acetate/s}$ (mCmol/Cmol)[c]	34.75 ± 0.41	37.44 ± 1.01*
$Y_{glycerol/s}$ (mCmol/Cmol)[d]	92.21 ± 5.73	66.31 ± 10.01*
$C_{ethanol,\ max}$ (mmol/L)[e]	153.45 ± 5.95	166.77 ± 2.64*
$C_{acetate,\ max}$ (mmol/L)[f]	11.58 ± 0.14	12.47 ± 0.47*
$C_{glycerol,\ max}$ (mmol/L)[g]	20.48 ± 1.27	14.73 ± 2.22*

The asterisk (*) indicates values significantly different from the control strain ($*p < 0.05$).
Results are represented as the average values ± SD of three independent biological replicates.
[a] Final biomass yield on substrate.
[b] Ethanol yield on glucose.
[c] Acetate yield on glucose.
[d] Glycerol yield on glucose.
[e] Maximal ethanol concentration.
[f] Maximal acetate concentration.
[g] Maximal glycerol concentration.

the N-linked glycans produced from yeast differ significantly from those found in humans (Hamilton and Gerngross, 2007). By disrupting the expression of *OCH1*, the gene responsible for endogenous glycosyltransferase activity, and subsequently introducing heterologous glycosylation enzymes, it could generate recombinant proteins with mammalian complex-type N-glycan structures (Jacobs et al., 2009). Truncating the open-reading-frame of *HOC1*, which alters cell-wall mannan, could enhance transformability and improve the secretion of recombinant proteins (Claes et al., 2024).

Moreover, *CWH41*, *PDI1*, and *SEC16* have been previously shown to enhance α-amylase production in *Saccharomyces cerevisiae*. For instance, overexpression of *CWH41* or *PDI1* using multicopy plasmids resulted in α-amylase production increases of 40% and 50%, respectively (Huang et al., 2018; Qi et al., 2020). Additionally, moderate overexpression of SEC16, driven by the strong GPD promoter, led to a two-fold increase in production (Bao et al., 2017). These studies utilized the AAC background strain (a strain of the CEN.PK family) with the CPOTud system, where α-amylase is expressed under the *TPI1* promoter in a *tpi1Δ* background strain. In our study, the starting strain CEN.PK 11C-GK1 was equipped with 14 integrated copies of the α-amylase gene, achieving production levels comparable to the AAC strain (Supplementary Fig. 1). This allowed us to compare α-amylase levels in parallel with our findings. Our study validated that upregulation of *CWH41*, *PDI1*, and *SEC16* enhanced amylase production by 25%, 51%, and 41%, respectively (Supplementary Fig. 13). Although the exact values differed, all three targets positively impacted α-amylase production across both backgrounds. Additionally, we compared α-amylase expression in another background strain, BY4742, in which α-amylase is expressed from a multicopy plasmid. This strain exhibited a 3.9-fold lower α-amylase level compared to CEN.PK 11C-GK1 (Supplementary Fig. 1). The effect of *IRE1*, another identified activation target, was examined in both BY4742 and CEN.PK 113C-GK1 strains. In the BY4742 strain, overexpression of *IRE1* did not significantly impact α-amylase production (Chen et al., 2022), whereas in CEN.PK 113C-GK1, it increased production by 30% (Supplementary Fig. 13). These results demonstrate that gene regulation may vary across background strains with different α-amylase expression levels.

Although engineering the protein secretory pathway has been proven to be a direct and efficient approach to enhance recombinant protein production in many cases, the limiting factors are also related to the central metabolic networks that provide building blocks, energy, and redox equivalents for protein production. Increased recombinant protein production is thought to impose a significant metabolic burden on cells by competing with native proteins for cellular resources (Dekel and Alon, 2005). Engineering of amino acid biosynthesis, lipid biosynthesis, cofactor biosynthesis, and oxygen sensing was reported to increase recombinant protein production yields (Chen et al., 2022; Huang et al., 2017; Martínez et al., 2015). From the CRISPRi library screening, 38 metabolism-related targets were verified and grouped to central carbon metabolism, amino acid and NAD biosynthesis (Fig. 3b). The central carbon metabolism comprises the core pathways in the cell, such as glycolysis, PPP, and TCA cycle, that convert substrates into energy, building blocks and products of biotechnological interest. *S. cerevisiae* displays a respiro-fermentative metabolism, also referred to as the Crabtree effect, in which cells predominantly consume glucose to produce ethanol via the fermentative pathway even under aerobic conditions (Pfeiffer and Morley, 2014). Similar examples of aerobic fermentation were also discovered in *E. coli* (van Hoek and Merks, 2012) and rapidly proliferating mammalian cells, e.g. lactic acid production in cancer cells (Vazquez and Oltvai, 2011). Studies have shown that fermentation exhibits a higher catalytic efficiency compared to respiration (Molenaar et al., 2009; Nilsson and Nielsen, 2016), enabling a greater rate of ATP production per unit of protein mass to meet the elevated energy requirements in strains with higher recombinant protein production. In the best performing strain AML, combinatorial engineering was applied to fine-tune gene expression of *LPD1*, *MDH1*, and *ACS1*, resulting in enhanced carbon flux to fermentation and a 3.18-fold α-amylase production, reaching 177.6 mg L^{-1} (Figs. 4 and 5c). Besides the enhanced carbon flux to ethanol production, FBA simulation also indicated an increased carbon flux to the PPP (Fig. 5c). Recombinant protein production at higher levels often induces oxidative stress on the host cells and demands extra reducing power to maintain cellular redox homeostasis (Heyland et al., 2011). Studies have shown that the overexpression of genes in the PPP and increased flux through the PPP could alleviate the metabolic burden and pose positive influence on production of heterologous proteins in different host organisms (Flores et al., 2004; Nocon et al., 2016). Targeting central carbon metabolism thus proves to be a useful strategy for metabolic engineering of recombinant protein production. For practical applications, the CRISPRi system may lead to additional metabolic burden and potential off-target effects. To mitigate these adverse effects, gene expression could be regulated by replacing the native promoter with a weaker alternative. In the best performing strain (AML strain), the mRNA levels of *LPD1*, *MDH1*, and *ACS1* were respectively decreased by 57%, 30%, and 22%, compared to the control strain (Supplementary Fig. 10). Based on previous research that assesses native promoter activity (Keren et al., 2013), a set of weaker promoters with varying transcriptional activities could be employed to lower gene expression.

Except for *LPD1*, *MDH1*, and *ACS1* genes, additional 9 novel metabolism-related targets were identified for enhanced α-amylase production through reverse engineering (Fig. 3e). These targets are involved in different roles, from reactions related to lipid biosynthesis and homeostasis (*LDH1*, *PAH1*, *ALE1*), amino acids biosynthesis (*GLN1*, *PRS3*, *ARO9*), *de novo* synthesis of GTP (*IMD4*), and TCA cycle (*IDP1*) (Supplementary Table 8). These genes and pathways present potential avenues for further investigation as additional targets to increase α-amylase production.

In summary, the genome-scale protein secretory model enables us to screen novel targets from metabolism and the protein secretory pathway for improved recombinant protein production in the yeast *S. cerevisiae*, via combination of targeted CRISPRi/a gRNAs library and high-throughput microfluidic-based screening. Furthermore, the combinatorial engineering of identified gene targets within central carbon metabolism provided informative data regarding the potential beneficial effects of enhanced fermentation for improved protein production. The general indication from these targets demonstrated the significance of optimizing cellular metabolism and potential bottlenecks that need to be overcome for recombinant protein production. Due to the strong conservation of the protein secretory pathway and central metabolism among eukaryal cells, our findings can be used as guidelines to rationally design cell factories in yeast and other eukaryal hosts for the production of biotherapeutic proteins.

4. Materials and methods

4.1. Prediction of engineering targets using the pcSecYeast model

The proteome-constrained secretory model for *S. cerevisiae*, pcSecYeast, served as the basis for target prediction in this study. For identification of potential overexpression and downregulation targets, an adapted FSEOF algorithm was used as detailed in the reference (Li et al., 2022). To mitigate the impact on growth and metabolic states, we confined our analysis to a specific growth rate window (0.25 h^{-1} to 0.3 h^{-1}). Within this range, we systematically reduced the growth rate while maximizing recombinant protein production, redirecting carbon flux from biomass to protein production. Given pcSecYeast's capability to estimate protein abundances, proteins exhibiting increased abundance with enhanced recombinant protein production were recognized as overexpression targets, while those with reduced abundance were considered downregulation targets.

To streamline experimental focus, we applied cutoffs to prioritize predicted targets. For overexpression targets: 1) Proteins consistently

increasing with enforced recombinant protein production, with a Spearman correlation score exceeding 0.9, received a priority score of 1; 2) Proteins meeting the criterion of priority score 1 and displaying an at least 1.2-fold abundance towards maximum recombinant protein production relative to maximum specific growth rate were assigned a priority score of 2; 3) Proteins with priority score 2 and exhibiting a comparable difference at high recombinant protein production compared with the PaxDb reference abundance were assigned a priority score of 3; 4) Proteins with priority score 3, which were neither subunits of complexes nor contained paralogs, received a priority score of 4. For downregulation targets: 1) Proteins consistently decreasing with enforced recombinant protein production, with a Spearman correlation score below −0.9, were given a priority score of −1; 2) Proteins meeting the criterion of priority score −1 and displaying a 0.83-fold abundance or lower towards maximum recombinant protein production relative to maximum specific growth rate received a priority score of −2; 3) Proteins with priority score −2 and showing a comparable difference at high recombinant protein production compared with the PaxDb reference abundance were assigned a priority score of −3; 4) Proteins with priority score −3, which were neither subunits of complexes nor contained paralogs, were given a priority score of −4.

To further refine the results, we performed a reference control simulation assessing protein abundance change with growth rate variation without recombinant protein production. Targets that also appeared in the reference control state received a score of 0.5 or −0.5, while those exclusive to the recombinant protein production case were awarded an extra 0.5 score for overexpression and −0.5 for downregulation. Priority scores close to 0 indicated proteins not identified as overexpression targets, positive higher priority scores suggested prioritization for overexpression, and negative lower priority scores indicated prioritization for downregulation.

Adhering to these criteria, we ranked and generated annotated tables for α-amylase production (Supplementary Table 1). When identifying common targets for further experiments, we focused on those with priority scores over 3 for overexpression and lower than −3 for downregulation.

4.2. Plasmids and strains

A full list of plasmids, *S. cerevisiae* strains, and primer sequences used in this study can be found in the Supplementary Tables 11, 12, and 13, respectively. The CEN.PK 11C-GK1 strain (*MATa his3-Δ1 MAL2-8c SUC2 Ty4-AlphaAmy-Ty4*) was utilized as host for strain construction. It contains 14 integrated copies of the *GPDp*-α-factor leader-α-amylase-*CYC1t* cassette containing the α-amylase gene from *Aspergillus oryzae* (Wang et al., 2019). The standard lithium acetate-based method was used for yeast transformation and library generation (Gietz and Woods, 2002). *E. coli* strain DH5α was used for plasmid propagation (Taylor et al., 1993). The integration of the dCas9-Mxi1 repressor and dCas9-VPR activator cassettes was performed with the help of the all-in-one plasmid pECAS9-gRNA-KanMX-XII-5, which encodes the Cas9 nuclease and a guide RNA for the chromosomal XII-5 locus (Chen et al., 2020; Jensen et al., 2014). The *TEF1p-dCas9-Mxi1-CYC1t* and *TEF1p-dCas9-VPR-CYC1t* expression cassettes were PCR amplified from Addgene plasmid #73796 (Smith et al., 2016) and #103140 (Ferreira et al., 2018), respectively. Around 500 bp of nucleotide sequences homologous to the upstream and downstream sequence of the XII-5 locus were amplified from genomic DNA of the CEN.PK 11C-GK1 strain and fused to the *TEF1p-dCas9-Mxi1-CYC1t* and *TEF1p-dCas9-VPR-CYC1t* cassettes to generate the repair fragments. The gene integration was performed by co-transformation of 300 ng of pECAS9-gRNA-KanMX-XII-5 vector and 600 ng of repair fragment into the CEN.PK 11C-GK1 strain to generate strains 11C-GK1-dCas9-Mxi1 and 11C-GK1-dCas9-VPR, respectively. The *csy4* gene was integrated into the 11C-GK1-dCas9-Mxi1 strain following the same method. The *PGK1p-csy4-ADH1t* cassette was amplified from plasmid pMG382-Csy4 (Otto et al., 2021) and integrated into chromosomal XI-3 locus by using the pECAS9-gRNA-KanMX-XI-3 vector (Chen et al., 2020) to generate strain 11C-GK1-dCas9-Mxi1-Csy4 (Supplementary Fig. 8a). The transformants were selected on SD-Ura plates containing 200 mg L^{-1} G418 (Formedium) and gene integration was confirmed by PCR analysis. The pECAS9-gRNA-kanMX-XII-5 or pECAS9-gRNA-kanMX-XI-3 plasmid was further removed by growing the transformants in SD-Ura medium for 24 h. The final transformants that had lost G418 resistance were selected for further experiments. Gene deletions were performed through homologous recombination by using *KanMX* as the selection marker, which was amplified from the pUG6 plasmid (Güldener et al., 1996). Gene-deletion cassettes consisted of the *KanMX* marker and the flanking homologous regions (around 500 bp each) of the target genes. After transformation, the transformants were selected on SD-Ura plates with 200 mg L^{-1} G418.

The double gRNAs plasmid (pMEL10-LPD1+MDH1) was constructed by Gibson assembly (Gibson et al., 2009). The gRNA scaffold sequence and the 28-bp Csy4 recognition sequence was PCR amplified from the pMCL8_28bp plasmid (Otto et al., 2021) using primers LPD1-Fwd and MDH1-Rev, which contain LPD1_gRNA and MDH1_gRNA, respectively. The pMEL10 backbone was PCR amplified from plasmid pMEL10 (Mans et al., 2015) with primers Scaffold-Fwd and SNRp-Rev. After PCR completion, 1 μl of DpnI was added to 50 μl PCR reaction and the mixture was incubated for 2 h at 37 °C. The two fragments were purified and assembled into plasmid pMEL10-LPD1+MDH1 via Gibson assembly (Supplementary Fig. 8b). The triple gRNAs plasmid (pMEL10-LPD1+MDH1+ACS1) was constructed via restriction digest and ligation reactions. The *EcoRI-SNR5p-ACS1_gRNA-CYC1t-BamHI* cassette was PCR amplified from pMEL10-ACS1 #1 plasmid using primers ACS1-EcoRI-Fwd and ACS1-BamHI-Rev, which included the *Eco*RI and *Bam*HI restriction site, respectively. The pMEL10-LPD1+MDH1 backbone was PCR amplified from plasmid pMEL10-LPD1+MDH1 with primers LM-BamHI-Fwd and LM-EcoRI-Rev, which contained *Bam*HI and *Ecor*RI restriction sites, respectively. The cassette and backbone were further digested with *Eco*RI and *Bam*HI restriction enzymes and ligated to form the pMEL10-LPD1+MDH1+ACS1 plasmid (Supplementary Fig. 8c).

4.3. Strain cultivation

E. coli strain DH5α was grown in LB medium (10 g L^{-1} peptone from casein, 10 g L^{-1} NaCl, 5 g L^{-1} yeast extract, pH set to 7.0 with NaOH) supplemented with 100 mg L^{-1} ampicillin at 37 °C. Yeast strains were grown in SD-Ura medium or 2 × SCAA medium without uracil and histidine at 30 °C according to the auxotrophic markers in cells. The SD-Ura medium contained 20 g L^{-1} glucose, 6.7 g L^{-1} yeast nitrogen base (YNB) without amino acids (Formedium), 770 mg L^{-1} complete supplement mixture (CSM) without uracil (CSM-Ura, Formedium). For the selection of cells containing the *KanMX* marker, 50 mg L^{-1} and 200 mg L^{-1} G418 were added to SD-Ura medium and plates, respectively. SD-Ura-His plates were used to select the correct transformants after library generation and contained 20 g L^{-1} glucose, 6.7 g L^{-1} YNB without amino acids (Formedium), 750 mg L^{-1} CSM without uracil and histidine (CSM-Ura-His, Formedium), 20 g L^{-1} agar. The protein production in tube or shake flask was carried out in SD-2 × SCAA medium without uracil and histidine as described previously (Wittrup and Benig, 1994), which contained, per liter, 20 g glucose, 6.9 g YNB without amino acids, 190 mg Arg, 400 mg Asp, 1260 mg Glu, 130 mg Gly, 290 mg Ile, 400 mg Leu, 440 mg Lys, 108 mg Met, 200 mg Phe, 220 mg Th, 40 mg Trp, 52 mg Tyr, 380 mg Val, 1 g bovine serum albumin (BSA), 5.4 g Na_2HPO_4, and 8.56 g $NaH_2PO_4{\cdot}H_2O$ (pH adjusted to 6.0 by NaOH).

4.4. Generation of yeast CRISPRi and CRISPRa libraries

The pcSecYeast model predicted 76 downregulation targets and 81 overexpression targets for the production of α-amylase. For each target, 10–14 gRNAs were designed using the online CHOPCHOP tool

(https://chopchop.cbu.uib.no/) (Labun et al., 2019). Each library contained 1000 gRNAs in total. The gRNAs oligo pools were ordered from Twist Bioscience (USA) and amplified with primers Oligo-Fwd and Oligo-Rev. These primers contained 100 bp of homologous arms flanking the gRNA region to increase the recombination efficiency. The protocol for amplifying the pooled oligo library was described previously (Joung et al., 2017). The backbone was amplified from plasmid pMEL10 using primer pairs pMEL10-Fwd/SNRp-Rev and Scaffold-Fwd/pMEL10-Rev, and further fused through fusion PCR. To remove the plasmid template, 1 μL of *Dpn*I was added to the finished 50 μL PCR reaction and the mixture was incubated at 37 °C for 2 h. For preparation of competent cells, the strains 11C-GK1-dCas9-Mxi1 and 11C-GK1-dCas9-VPR were cultured in 20 mL of fresh medium until OD_{600} reaching 1.0. Subsequently, approximately 2 μg of the fused backbone and 1 μg of the PCR-amplified CRISPRi gRNA pool or CRISPRa gRNA pool were used to transform the 11C-GK1-dCas9-Mxi1 and 11C-GK1-dCas9-VPR competent cells, respectively. The number of transformants was determined by plating 10-fold serial dilutions of transformed cells on SD-Ura-His plates at 30 °C. Colonies were counted after 2–3 days. The CRISPRi library contained 240,000 clones, and CRISPRa library contained 280,000 clones. To estimate the number of effective clones in the library, excluding those not containing a gRNA, we subjected 20 random clones per library to plasmid sequencing (Supplementary Tables 4 and 5).

4.5. Microfluidic device setup

The microfluidic devices were manufactured by Wunderlichips GmbH (Switzerland) according to the design of Brower et al. (2020b). In order to form the water-in-oil-in-water (WOW) double emulsion (DE) droplets, the surface wettability of the microfluidic channels needed to be selectively modified (Brower et al., 2020b). To this end, the microfluidic devices were first baked at 65 °C for 2–3 days to maximize their hydrophobicity. Before the generation of DEs droplets, the second intersection and the outlet channel of the baked microfluidic devices was selectively treated with air plasma (BatchTop RIE, Plasma Therm) at 250 W for 5 min, while the inlets were covered by Kapton tape. The air plasma followed this flow path to switch the outlet path to hydrophilic wettability while retaining hydrophobicity at the inlet path. After the plasma treatment, the tap was removed, and the channels were immediately flushed with distilled water. The goal of this procedure was to maintain high hydrophobicity at the first intersection of the chip (water-in-oil droplet generation) and a high hydrophilicity at the second intersection (water-in-oil-in-water droplet generation). This wettability pattern inside the microfluidic devices can last for 3–4 h. The microfluidic device was connected to three syringe pumps (Fluigent) for cell suspension, oil, and outer sheath solutions via PPEK tubing (0.01 inch for inner diameter and 1/32 inch for outer diameter, Fisher Scientific). Generation of DE droplets was monitored through the stereoscope (Mitutoyo) and high-speed CMOS camera (Pixelink) (Supplementary Fig. 3).

4.6. Encapsulation of yeast library in DE droplets

The yeast library was cultivated overnight in 20 mL of SD-2 × SCAA medium and washed once with sterile distilled water. Ten OD_{600} of cells were resuspended in 5 mL of SD-2 × SCAA medium and ultra-sonicated for 4 × 10 s at 10% of amplitude (Branson Ultrasonics) to separate cell clumps. Before loading to the microfluidic device, cells were mixed 1:1 with 200 μg mL^{-1} BODIPY labeled DQ starch substrate from the Ultra Amylase Assay Kit (Thermo Scientific). The oil phase consisted of 2.2% Ionic PEG-Krytox (Costenoble) and HEF 7500 (Fluigent). The outer sheath contained SD-2 × SCAA medium, 10% Pluronic F68 (Gibco), 1% Tween-20 (Sigma-Aldrich), 100 mg L^{-1} ampicillin (Amp, Sigma-Aldrich), and 25 mg L^{-1} chloramphenicol (CAM, Sigma-Aldrich) (Brower et al., 2020b). Lower flow rates (2.6:4.8:42 μL min^{-1}, cell/oil/outer sheath) were applied to lessen the cell shear stress. DE droplets were collected in a 100-mL shake flask filled with 10 mL of outer sheath. Subsequently, DEs were incubated at 30 °C, 80 rpm agitation for 3 h prior to be analyzed using a FACS SH800 (Sony).

4.7. FACS analysis and sorting of DE droplets

Prior to FACS analysis, 100 μL of DE droplets were gently aspirated from the bottom of the shake flask and diluted in 500 μL of ClearSort FACS sheath fluid (Sony) containing 1% Tween-20, 100 mg L^{-1} Amp and 25 mg L^{-1} CAM. The 488-nm laser and a 130-μm nozzle were used for sorting of the DE droplets. The flow and thresholding parameters were set as follows: trigger, FSC; threshold, 0.67%; FSC gain, 1; SSC gain, 28%; 488 nm laser gain, 28%; sample pressure, 9 psi until DE events, 4–5 psi during sorting. Sample pressure was adjusted to achieve below 1000 events/sec for sorting purity (Brower et al., 2020b). Around 100,000 DE droplets (100-fold of library size) were screened to achieve adequate coverage. DE droplets were first gated on the FSC-H *vs.* FSC-W profile for large particle analysis, and subsequently gated on the 520/50 nm filter. Based on the fluorescence distribution, the top 0.5–5% of the droplets were sorted and collected in a FACS 12 × 75 mm tube filled with 5 mL of FACS diluent buffer. After sorting was completed, the sorted droplets were centrifuged at 2000 g for 5 min and then resuspended in fresh SD-2 × SCAA medium. Afterwards, they were spread onto starch agar plates. The droplets broke during the centrifugation and plating steps. The plates were then incubated at 30 °C for 3–5 days until single colonies were formed. Starch agar plate contained 1% starch (Sigma-Aldrich), 100 mg L^{-1} Amp, 25 mg L^{-1} CAM, and 2% agar (Sigma-Aldrich) in SD-2 × SCAA medium.

4.8. Quantification of α-amylase

The single colonies from the DE droplet sorting screening were inoculated in 1 mL SD-2 × SCAA medium overnight at 30 °C with 200 rpm agitation. The preculture was diluted to an initial OD_{600} of 0.05 in 2.5 mL of SD-2 × SCAA medium within 14-mL culture tubes. After 96 h of cultivation, the supernatant was collected after centrifugation at 4 °C, 4000 rpm for 5 min. The α-amylase activity was quantified using the α-amylase assay kit (K-CERA, Megazyme) at 40 °C for 10 min according to the manufacturer's instructions. The *A. oryzae* α-amylase (Sigma-Aldrich) was applied as a standard. The α-amylase concentration was converted with 69.6 U mg^{-1} as the protein conversion coefficient.

4.9. Verification of the sorted strains

Compared to the control strain, an α-amylase titer ≥1.2-fold was set as threshold to select strains for further analysis. To determine the targeted genes, the plasmids were extracted from these yeast strains using the Zymoprep Yeast Plasmid Miniprep II kit (ZYMO Research) and sequenced via Eurofins Genomics. The verified gene targets were analyzed for GSEA via the Database for Annotation, Visualization and Integrated Discovery platform (DAVID, https://david.ncifcrf.gov/) and the Gene Ontology Slim Term Mapper on *Saccharomyces* Genome Database (SGD, https://www.yeastgenome.org/goSlimMapper). The library before sorting was used as a reference. For reverse metabolic engineering, the top 14 yeast strains with improved α-amylase production were selected. The plasmids were extracted from these strains and used to re-transform the 11C-GK1-dCas9-Mxi1 strain. The α-amylase production was quantified as described above.

4.10. Determination of biomass and extracellular metabolites

For the shake-flasks cultivation, precultures were prepared using 25 mL of SD-2 × SCAA medium with an initial OD_{600} of 0.1. The biomass was determined by OD_{600}. OD_{600} were measured by spectrophotometry (Thermo Scientific) and converted to dry cell weight (DCW) as grams by

a multiplication factor of 0.6524 g DCW/OD_{600}. This multiplication factor was calculated from the calibration curves of DCW versus OD_{600} (Chen et al., 2017). To measure the extracellular metabolites, 200 μL of supernatant was collected after centrifugation at 4 °C, 14,000 rpm for 10 min, and immediately frozen at −20 °C. The extracellular glucose, ethanol, acetate, and glycerol concentrations were analyzed on a Dionex Ultimate 3000 HPLC (Thermo Fisher Scientific) equipped with an Aminex HPX-87H column (Bio-Rad). The mobile phase for the column was 5 mM H_2SO_4 and the column was kept at 45 °C with a flow rate of 0.6 mL min^{-1}.

4.11. SDS-PAGE

The control and AML strain were grown in 2.5 mL of SD-2 × SCAA medium without BSA with an initial OD_{600} of 0.1 for 96 h. The supernatant was collected after centrifugation at 4 °C, 4000 rpm for 5 min and concentrated 50-fold using the protein concentrators PES (10K MW cutoff, Thermo Scientific). The concentrated supernatant was mixed with 4 × NuPAGE LDS sample buffer (Thermo Scientific) and 10 × NuPAGE sample reducing agent (Thermo Scientific). The mixture was boiled at 95 °C for 5 min and loaded onto a 4–20% precast polyacrylamide gel (Mini-PROTEAN TGX Stain-Free Protein Gels, Bio-Rad). After electrophoresis, the gel was imaged using the Gel Doc EZ imaging system (BioRad).

4.12. Quantitative real-time PCR analysis

The control and AML strain were grown in 25 mL of SD-2 × SCAA medium with an initial OD_{600} of 0.1. Around 10 OD_{600} of cells were taken at mid exponential phase ($OD_{600} \approx 1.5$). Total RNA was extracted using the RNeasy Mini Kit (Qiagen) according to the manufacturer's instructions. First-strand cDNA was synthesized from 500 ng of total RNA using a QuantiTect Reverse Transcription kit (QIAGEN). The qPCR assay was performed using the DyNAmo Flash SYBR Green qPCR kit (Thermo Fisher Scientific) and the Mx3005P QPCR system (Agilent Technologies). The *ACT1* gene was used as a reference gene to normalize RNA levels. The $2^{-\Delta\Delta CT}$ method was used to quantify the relative transcription levels.

4.13. Flux simulation of engineered strain

The flux distribution for engineered strains was simulated using flux balance analysis (FBA) with the pcSecYeast model. Condition-specific models for engineered strains were created by incorporating and constraining the models with experimental measurements of metabolite exchange rates. For the downregulation of the *LPD1*, *MDH1*, and *ACS1* genes in the AML strain, the flux for the corresponding reactions was constrained according to reference control flux simulations. MATLAB R2022b (MathWorks Inc.) with IBM CPLEX solver was employed for simulations.

4.14. Statistical analysis

Data were presented as mean ± standard deviation (SD) and significant differences were determined by a two-tailed student *t*-test. As identical procedures were used to determine the parameters, equal variance was applied to student *t*-tests. Unless specified explicitly, three biological replicates were included in the data analysis. The p value < 0.05 was indicated as the statistical significance unless explicitly stated.

CRediT authorship contribution statement

Xin Chen: Writing – review & editing, Writing – original draft, Visualization, Validation, Resources, Methodology, Investigation, Formal analysis, Conceptualization. **Feiran Li:** Writing – review & editing, Writing – original draft, Resources, Methodology, Formal analysis. **Xiaowei Li:** Writing – review & editing, Investigation, Formal analysis, Conceptualization. **Maximilian Otto:** Writing – review & editing, Methodology. **Yu Chen:** Writing – review & editing, Investigation. **Verena Siewers:** Writing – review & editing, Supervision, Project administration, Conceptualization.

Declaration of competing interests

The authors declare that there are no competing interests.

Acknowledgements

This work was supported by grants from the VINNOVA center CellNova (2017–02105) and Novo Nordisk Foundation (NNF10CC1016517). The authors would like to acknowledge the Nanofabrication Laboratory (Myfab) at the Chalmers University of Technology for their assistance with the air plasma treatment, and the Mass Spectrometry Infrastructure (CMSI) at the Chalmers University of Technology for their support with measuring extracellular metabolites.

Appendix A. Supplementary data

Supplementary data to this article can be found online at https://doi.org/10.1016/j.ymben.2024.11.010.

Data availability

Data will be made available on request.

References

Anderson, D.A., Voigt, C.A., 2021. Competitive dCas9 binding as a mechanism for transcriptional control. Mol. Syst. Biol. 17, e10512.
Bao, J., Huang, M., Petranovic, D., Nielsen, J., 2017. Moderate expression of SEC16 increases protein secretion by *Saccharomyces cerevisiae*. Appl. Environ. Microbiol. 83, e03400–e03416.
Baret, J.-C., Miller, O.J., Taly, V., Ryckelynck, M., El-Harrak, A., Frenz, L., Rick, C., Samuels, M.L., Hutchison, J.B., Agresti, J.J., Link, D.R., Weitz, D.A., Griffiths, A.D., 2009. Fluorescence-activated droplet sorting (FADS): efficient microfluidic cell sorting based on enzymatic activity. Lab Chip 9, 1850–1858.
Bendixen, L., Jensen, T.I., Bak, R.O., 2023. CRISPR-Cas-mediated transcriptional modulation: the therapeutic promises of CRISPRa and CRISPRi. Mol. Ther. 31, 1920–1937.
Brower, K.K., Carswell-Crumpton, C., Klemm, S., Cruz, B., Kim, G., Calhoun, S.G.K., Nichols, L., Fordyce, P.M., 2020a. Double emulsion flow cytometry with high-throughput single droplet isolation and nucleic acid recovery. Lab Chip 20, 2062–2074.
Brower, K.K., Khariton, M., Suzuki, P.H., Still, C.I.I., Kim, G., Calhoun, S.G.K., Qi, L.S., Wang, B., Fordyce, P.M., 2020b. Double emulsion picoreactors for high-throughput single-cell encapsulation and phenotyping via FACS. Anal. Chem. 92, 13262–13270.
Campbell, K., Xia, J., Nielsen, J., 2017. The Impact of systems biology on bioprocessing. Trends Biotechnol. 35, 1156–1168.
Cantoia, A., Aguilar Lucero, D., Ceccarelli, E.A., Rosano, G.L., 2021. From the notebook to recombinant protein production in *Escherichia coli*: design of expression vectors and gene cloning. Methods Enzymol. 659, 19–35.
Cardiff, R.A.L., Carothers, J.M., Zalatan, J.G., Sauro, H.M., 2024. Systems-level modeling for CRISPR-based metabolic engineering. ACS Synth. Biol. 13, 2643–2652.
Chan, H.F., Ma, S., Tian, J., Leong, K.W., 2017. High-throughput screening of microchip-synthesized genes in programmable double-emulsion droplets. Nanoscale 9, 3485–3495.
Chen, X., Bisschops, M.M.M., Agarwal, N.R., Ji, B., Shanmugavel, K.P., Petranovic, D., 2017. Interplay of energetics and ER stress exacerbates alzheimer's amyloid-β (aβ) toxicity in yeast. Front. Mol. Neurosci. 10.
Chen, X., Ji, B., Hao, X., Li, X., Eisele, F., Nyström, T., Petranovic, D., 2020. FMN reduces Amyloid-β toxicity in yeast by regulating redox status and cellular metabolism. Nat. Commun. 11, 867.
Chen, X., Li, X., Ji, B., Wang, Y., Ishchuk, O.P., Vorontsov, E., Petranovic, D., Siewers, V., Engqvist, M.K.M., 2022. Suppressors of amyloid-β toxicity improve recombinant protein production in yeast by reducing oxidative stress and tuning cellular metabolism. Metab. Eng. 72, 311–324.
Cho, J.S., Kim, G.B., Eun, H., Moon, C.W., Lee, S.Y., 2022. Designing microbial cell factories for the production of chemicals. JACS Au 2, 1781–1799.
Claes, K., Van Herpe, D., Vanluchene, R., Roels, C., Van Moer, B., Wyseure, E., Vandewalle, K., Eeckhaut, H., Yilmaz, S., Vanmarcke, S., Çıtak, E., Fijalkowska, D., Grootaert, H., Lonigro, C., Meuris, L., Michielsen, G., Naessens, J., van Schie, L., De Rycke, R., De Bruyne, M., Borghgraef, P., Callewaert, N., 2024. OPENPichia: licence-

free Komagataella phaffii chassis strains and toolkit for protein expression. Nat. Microbiol. 9, 864–876.
Dekel, E., Alon, U., 2005. Optimality and evolutionary tuning of the expression level of a protein. Nature 436, 588–592.
Ding, Q., Diao, W., Gao, C., Chen, X., Liu, L., 2020. Microbial cell engineering to improve cellular synthetic capacity. Biotechnol. Adv. 45, 107649.
Evers, B., Jastrzebski, K., Heijmans, J.P.M., Grernrum, W., Beijersbergen, R.L., Bernards, R., 2016. CRISPR knockout screening outperforms shRNA and CRISPRi in identifying essential genes. Nat. Biotechnol. 34, 631–633.
Ferreira, R., Skrekas, C., Hedin, A., Sánchez, B.J., Siewers, V., Nielsen, J., David, F., 2019. Model-assisted fine-tuning of central carbon metabolism in yeast through dCas9-based regulation. ACS Synth. Biol. 8, 2457–2463.
Ferreira, R., Skrekas, C., Nielsen, J., David, F., 2018. Multiplexed CRISPR/Cas9 genome editing and gene regulation using csy4 in *Saccharomyces cerevisiae*. ACS Synth. Biol. 7, 10–15.
Flores, S., de Anda-Herrera, R., Gosset, G., Bolívar, F.G., 2004. Growth-rate recovery of *Escherichia coli* cultures carrying a multicopy plasmid, by engineering of the pentose-phosphate pathway. Biotechnol. Bioeng. 87, 485–494.
Geva, Y., Schuldiner, M., 2014. The back and forth of cargo exit from the endoplasmic reticulum. Curr. Biol. 24, R130–R136.
Gibson, D.G., Young, L., Chuang, R.-Y., Venter, J.C., Hutchison, C.A., Smith, H.O., 2009. Enzymatic assembly of DNA molecules up to several hundred kilobases. Nat. Methods 6, 343–345.
Gietz, R.D., Woods, R.A., 2002. Transformation of yeast by lithium acetate/single-stranded carrier DNA/polyethylene glycol method. Methods Enzymol. 350, 87–96.
Gilbert, L.A., Horlbeck, M.A., Adamson, B., Villalta, J.E., Chen, Y., Whitehead, E.H., Guimaraes, C., Panning, B., Ploegh, H.L., Bassik, M.C., Qi, L.S., Kampmann, M., Weissman, J.S., 2014. Genome-scale CRISPR-mediated control of gene repression and activation. Cell 159, 647–661.
Gupta, V., Sengupta, M., Prakash, J., Tripathy, B.C., 2017. Production of recombinant pharmaceutical proteins. In: Gupta, V., Sengupta, M., Prakash, J., Tripathy, B.C. (Eds.), Basic and Applied Aspects of Biotechnology. Springer, Singapore, pp. 77–101. Singapore.
Gutierrez, J.M., Feizi, A., Li, S., Kallehauge, T.B., Hefzi, H., Grav, L.M., Ley, D., Baycin Hizal, D., Betenbaugh, M.J., Voldborg, B., Faustrup Kildegaard, H., Min Lee, G., Palsson, B.O., Nielsen, J., Lewis, N.E., 2020. Genome-scale reconstructions of the mammalian secretory pathway predict metabolic costs and limitations of protein secretion. Nat. Commun. 11, 68.
Güldener, U., Heck, S., Fielder, T., Beinhauer, J., Hegemann, J.H., 1996. A new efficient gene disruption cassette for repeated use in budding yeast. Nucleic Acids Res. 24, 2519–2524.
Hamilton, S.R., Gerngross, T.U., 2007. Glycosylation engineering in yeast: the advent of fully humanized yeast. Curr. Opin. Biotechnol. 18, 387–392.
Hetz, C., Papa, F.R., 2018. The unfolded protein response and cell fate control. Mol. Cell 69, 169–181.
Heyland, J., Fu, J., Blank, L.M., Schmid, A., 2011. Carbon metabolism limits recombinant protein production in *Pichia pastoris*. Biotechnol. Bioeng. 108, 1942–1953.
Huang, M., Bai, Y., Sjostrom, S.L., Hallström, B.M., Liu, Z., Petranovic, D., Uhlén, M., Joensson, H.N., Andersson-Svahn, H., Nielsen, J., 2015. Microfluidic screening and whole-genome sequencing identifies mutations associated with improved protein secretion by yeast. Proc. Natl. Acad. Sci. U.S.A. 112, E4689–E4696.
Huang, M., Bao, J., Hallström, B.M., Petranovic, D., Nielsen, J., 2017. Efficient protein production by yeast requires global tuning of metabolism. Nat. Commun. 8, 1131.
Huang, M., Wang, G., Qin, J., Petranovic, D., Nielsen, J., 2018. Engineering the protein secretory pathway of *Saccharomyces cerevisiae* enables improved protein production. Proc. Natl. Acad. Sci. U.S.A. 115, E11025–e11032.
Irani, Z.A., Kerkhoven, E.J., Shojaosadati, S.A., Nielsen, J., 2016. Genome-scale metabolic model of *Pichia pastoris* with native and humanized glycosylation of recombinant proteins. Biotechnol. Bioeng. 113, 961–969.
Jacobs, P.P., Geysens, S., Vervecken, W., Contreras, R., Callewaert, N., 2009. Engineering complex-type N-glycosylation in *Pichia pastoris* using GlycoSwitch technology. Nat. Protoc. 4, 58–70.
Jensen, N.B., Strucko, T., Kildegaard, K.R., David, F., Maury, J., Mortensen, U.H., Forster, J., Nielsen, J., Borodina, I., 2014. EasyClone: method for iterative chromosomal integration of multiple genes *Saccharomyces cerevisiae*. FEMS Yeast Res. 14, 238–248.
Johansson, S.A., Dulermo, T., Jann, C., Smith, J.D., Pryszlak, A., Pignede, G., Schraivogel, D., Colavizza, D., Desfougères, T., Rave, C., Farwick, A., Merten, C.A., Roy, K.R., Wei, W., Steinmetz, L.M., 2023. Large scale microfluidic CRISPR screening for increased amylase secretion in yeast. Lab Chip 23, 3704–3715.
Joung, J., Konermann, S., Gootenberg, J.S., Abudayyeh, O.O., Platt, R.J., Brigham, M.D., Sanjana, N.E., Zhang, F., 2017. Genome-scale CRISPR-Cas9 knockout and transcriptional activation screening. Nat. Protoc. 12, 828–863.
Jung, S.-W., Yeom, J., Park, J.S., Yoo, S.M., 2021. Recent advances in tuning the expression and regulation of genes for constructing microbial cell factories. Biotechnol. Adv. 50, 107767.
Keren, L., Zackay, O., Lotan-Pompan, M., Barenholz, U., Dekel, E., Sasson, V., Aidelberg, G., Bren, A., Zeevi, D., Weinberger, A., Alon, U., Milo, R., Segal, E., 2013. Promoters maintain their relative activity levels under different growth conditions. Mol. Syst. Biol. 9, 701.
Krambeck, F.J., Betenbaugh, M.J., 2005. A mathematical model of N-linked glycosylation. Biotechnol. Bioeng. 92, 711–728.
Labun, K., Montague, T.G., Krause, M., Torres Cleuren, Y.N., Tjeldnes, H., Valen, E., 2019. CHOPCHOP v3: expanding the CRISPR web toolbox beyond genome editing. Nucleic Acids Res. 47, W171–W174.
Legut, M., Gajic, Z., Guarino, M., Daniloski, Z., Rahman, J.A., Xue, X., Lu, C., Lu, L., Mimitou, E.P., Hao, S., Davoli, T., Diefenbach, C., Smibert, P., Sanjana, N.E., 2022. A genome-scale screen for synthetic drivers of T cell proliferation. Nature 603, 728–735.
Li, F., Chen, Y., Qi, Q., Wang, Y., Yuan, L., Huang, M., Elsemman, I.E., Feizi, A., Kerkhoven, E.J., Nielsen, J., 2022. Improving recombinant protein production by yeast through genome-scale modeling using proteome constraints. Nat. Commun. 13, 2969.
Lin, Y., Feng, Y., Zheng, L., Zhao, M., Huang, M., 2023. Improved protein production in yeast using cell engineering with genes related to a key factor in the unfolded protein response. Metab. Eng. 77, 152–161.
Liu, Z., Tyo, K.E., Martínez, J.L., Petranovic, D., Nielsen, J., 2012. Different expression systems for production of recombinant proteins in Saccharomyces cerevisiae. Biotechnol. Bioeng. 109, 1259–1268.
Madhavan, A., Arun, K.B., Sindhu, R., Krishnamoorthy, J., Reshmy, R., Sirohi, R., Pugazhendi, A., Awasthi, M.K., Szakacs, G., Binod, P., 2021. Customized yeast cell factories for biopharmaceuticals: from cell engineering to process scale up. Microb. Cell Factories 20, 124.
Mans, R., van Rossum, H.M., Wijsman, M., Backx, A., Kuijpers, N.G., van den Broek, M., Daran-Lapujade, P., Pronk, J.T., van Maris, A.J., Daran, J.M., 2015. CRISPR/Cas9: a molecular Swiss army knife for simultaneous introduction of multiple genetic modifications in *Saccharomyces cerevisiae*. FEMS Yeast Res. 15.
Martínez, J.L., Liu, L., Petranovic, D., Nielsen, J., 2015. Engineering the oxygen sensing regulation results in an enhanced recombinant human hemoglobin production by *Saccharomyces cerevisiae*. Biotechnol. Bioeng. 112, 181–188.
Mastrobattista, E., Taly, V., Chanudet, E., Treacy, P., Kelly, B.T., Griffiths, A.D., 2005. High-throughput screening of enzyme libraries: in vitro evolution of a beta-galactosidase by fluorescence-activated sorting of double emulsions. Chem. Biol. 12, 1291–1300.
Molenaar, D., van Berlo, R., de Ridder, D., Teusink, B., 2009. Shifts in growth strategies reflect tradeoffs in cellular economics. Mol. Syst. Biol. 5, 323.
Momen-Roknabadi, A., Oikonomou, P., Zegans, M., Tavazoie, S., 2020. An inducible CRISPR interference library for genetic interrogation of *Saccharomyces cerevisiae* biology. Commun. Biol. 3, 723.
Mukherjee, V., Lind, U., St Onge, R.P., Blomberg, A., Nygård, Y., 2021. A CRISPR interference screen of essential genes reveals that proteasome regulation dictates acetic acid tolerance in *Saccharomyces cerevisiae*. mSystems 6, e0041821.
Nielsen, J., 2017. Systems biology of metabolism. Annu. Rev. Biochem. 86, 245–275.
Nilsson, A., Nielsen, J., 2016. Metabolic trade-offs in yeast are caused by F1F0-ATP synthase. Sci. Rep. 6, 22264.
Nocon, J., Steiger, M., Mairinger, T., Hohlweg, J., Rußmayer, H., Hann, S., Gasser, B., Mattanovich, D., 2016. Increasing pentose phosphate pathway flux enhances recombinant protein production in *Pichia pastoris*. Appl. Microbiol. Biotechnol. 100, 5955–5963.
Nocon, J., Steiger, M.G., Pfeffer, M., Sohn, S.B., Kim, T.Y., Maurer, M., Rußmayer, H., Pflügl, S., Ask, M., Haberhauer-Troyer, C., Ortmayr, K., Hann, S., Koellensperger, G., Gasser, B., Lee, S.Y., Mattanovich, D., 2014. Model based engineering of *Pichia pastoris* central metabolism enhances recombinant protein production. Metab. Eng. 24, 129–138.
Ottenheim, C., Nawrath, M., Wu, J.C., 2018. Microbial mutagenesis by atmospheric and room-temperature plasma (ARTP): the latest development. Bioresour Bioproc. 5, 12.
Otto, M., Skrekas, C., Gossing, M., Gustafsson, J., Siewers, V., David, F., 2021. Expansion of the yeast modular cloning toolkit for CRISPR-based applications, genomic integrations and combinatorial libraries. ACS Synth. Biol. 10, 3461–3474.
Ow, D.S., Oh, M.K., Chiang, C.J., Chao, Y.P., 2021. Editorial: technological advances improving recombinant protein production in bacteria. Front. Microbiol. 12, 729472.
Perez-Pinera, P., Kocak, D.D., Vockley, C.M., Adler, A.F., Kabadi, A.M., Polstein, L.R., Thakore, P.I., Glass, K.A., Ousterout, D.G., Leong, K.W., Guilak, F., Crawford, G.E., Reddy, T.E., Gersbach, C.A., 2013. RNA-guided gene activation by CRISPR-Cas9–based transcription factors. Nat. Methods 10, 973–976.
Pfeiffer, T., Morley, A., 2014. An evolutionary perspective on the Crabtree effect. Front. Mol. Biosci. 1, 17.
Przybyla-Zawislak, B., Gadde, D.M., Ducharme, K., McCammon, M.T., 1999. Genetic and biochemical interactions involving tricarboxylic acid cycle (TCA) function using a collection of mutants defective in all TCA cycle genes. Genetics 152, 153–166.
Qi, Q., Li, F., Yu, R., Engqvist, M.K.M., Siewers, V., Fuchs, J., Nielsen, J., 2020. Different routes of protein folding contribute to improved protein production in *Saccharomyces cerevisiae*. mBio 11. https://doi.org/10.1128/mbio.02743-20.
Rakestraw, J.A., Sazinsky, S.L., Piatesi, A., Antipov, E., Wittrup, K.D., 2009. Directed evolution of a secretory leader for the improved expression of heterologous proteins and full-length antibodies in *Saccharomyces cerevisiae*. Biotechnol. Bioeng. 103, 1192–1201.
Silvis, M.R., Rajendram, M., Shi, H., Osadnik, H., Gray, A.N., Cesar, S., Peters, J.M., Hearne, C.C., Kumar, P., Todor, H., Huang, K.C., Gross, C.A., 2021. Morphological and transcriptional responses to CRISPRi knockdown of essential genes in *Escherichia coli*. mBio 12, e0256121.
Smith, J.D., Suresh, S., Schlecht, U., Wu, M., Wagih, O., Peltz, G., Davis, R.W., Steinmetz, L.M., Parts, L., St Onge, R.P., 2016. Quantitative CRISPR interference screens in yeast identify chemical-genetic interactions and new rules for guide RNA design. Genome Biol. 17, 45.
Tangphatsornruang, S., Naconsie, M., Thammarongtham, C., Narangajavana, J., 2005. Isolation and characterization of an alpha-amylase gene in cassava (Manihot esculenta). Plant Physiol. Biochem. 43, 821–827.

Taylor, R.G., Walker, D.C., McInnes, R.R., 1993. *E. coli* host strains significantly affect the quality of small scale plasmid DNA preparations used for sequencing. Nucleic Acids Res. 21, 1677–1678.
Tran, T.M., Lan, F., Thompson, C.S., Abate, A.R., 2013. From tubes to drops: droplet-based microfluidics for ultrahigh-throughput biology. J. Phys. Appl. Phys. 46, 114004.
van Hoek, M.J., Merks, R.M., 2012. Redox balance is key to explaining full vs. partial switching to low-yield metabolism. BMC Syst. Biol. 6, 22.
Vazquez, A., Oltvai, Z.N., 2011. Molecular crowding defines a common origin for the warburg effect in proliferating cells and the lactate threshold in muscle physiology. PLoS One 6, e19538.
Vieira Gomes, A.M., Souza Carmo, T., Silva Carvalho, L., Mendonça Bahia, F., Parachin, N.S., 2018. Comparison of yeasts as hosts for recombinant protein production. Microorganisms 6.
Wang, G., Björk, S.M., Huang, M., Liu, Q., Campbell, K., Nielsen, J., Joensson, H.N., Petranovic, D., 2019. RNAi expression tuning, microfluidic screening, and genome recombineering for improved protein production in *Saccharomyces cerevisiae*. Proc. Natl. Acad. Sci. U.S.A. 116, 9324–9332.
Wang, G., Huang, M., Nielsen, J., 2017. Exploring the potential of *Saccharomyces cerevisiae* for biopharmaceutical protein production. Curr. Opin. Biotechnol. 48, 77–84.
Wittrup, K.D., Benig, V., 1994. Optimization of amino acid supplements for heterologous protein secretion in *Saccharomyces cerevisiae*. Biotechnol. Tech. 8, 161–166.
Wu, G., 2009. Amino acids: metabolism, functions, and nutrition. Amino Acids 37, 1–17.
Ye, L., Park, J.J., Peng, L., Yang, Q., Chow, R.D., Dong, M.B., Lam, S.Z., Guo, J., Tang, E., Zhang, Y., Wang, G., Dai, X., Du, Y., Kim, H.R., Cao, H., Errami, Y., Clark, P., Bersenev, A., Montgomery, R.R., Chen, S., 2022. A genome-scale gain-of-function CRISPR screen in CD8 T cells identifies proline metabolism as a means to enhance CAR-T therapy. Cell Metabol. 34, 595–614.e14.
Zhang, C., Hua, Q., 2015. Applications of genome-scale metabolic models in biotechnology and systems medicine. Front. Physiol. 6, 413.